Energy & Environmental Science

Principle in Developing Novel Fluorinated Sulfone Electrolyte for High Voltage Lithium-ion Batteries

Journal:	*Energy & Environmental Science*
Manuscript ID	EE-COM-12-2020-003890.R1
Article Type:	Communication
Date Submitted by the Author:	20-Feb-2021
Complete List of Authors:	Su, Chi-Cheung; Argonne National Laboratory, He, Meinan; Argonne National Laboratory, Chemical Science & Engineering Shi, Jiayan; University of California Riverside, Chemical and Environmental Engineering; Argonne National Laboratory, Chemical Science and Engineering Amine, Rachid; University of Illinois at Chicago, Chemical Engineering; Argonne National Laboratory, Materials Science Division Yu, Zhou; Argonne National Lab, MSD Cheng, Lei; Argonne National Laboratory, Materials Science Division Guo, Juchen; University of California at Riverside, Chemical and Environmental Engineering Amine, Khalil; Argonne National Laboratory,

Principle in Developing Novel Fluorinated Sulfone Electrolyte for High Voltage Lithium-ion Batteries

Chi-Cheung Su,[a*] Meinan He,[a*] Jiayan Shi,[a,b] Rachid Amine,[c] Zhou Yu,[c] Lei Cheng,[c] Juchen Guo,[b] and Khalil Amine[a,d*]

[a] Chemical Sciences and Engineering Division, Argonne National Laboratory, 9700 S. Cass Avenue, Lemont, IL 60439, USA

[b] Department of Chemical and Environmental Engineering, University of California-Riverside, Riverside, CA 92521, USA

[c] Materials Science Division, Argonne National Laboratory, 9700 S. Cass Avenue, Lemont, IL 60439, USA

[d] Material Science and Engineering, Stanford University, Stanford, CA 94305, USA

E-mail: amine@anl.gov; csu@anl.gov; mhe@wpi.edu

ABSTRACT

A new class of fluorinated sulfones, *β*-fluorinated sulfones, were designed and synthesized as electrolyte solvents for high voltage lithium-ion batteries. While the oxidation potential of *β*-fluorinated sulfones is slightly lower than that of *α*-fluorinated sulfones, it is still significantly higher than the oxidation potential of regular sulfones, which already possess fairly high anodic stability. However, *β*-fluorinated sulfones exhibit a significant decrease in reduction potential compared to α-fluorinated sulfones, rendering them more stable towards graphite anodes. Moreover, the reduced lithium solvating power of *β*-fluorinated sulfones compared to regular sulfones mitigates the transition metal dissolution of cathodes. Taken together, these middle ground properties of *β*-fluorinated sulfone-based electrolytes enable the very stable long-term cycling of graphite||$LiNi_{0.6}Co_{0.2}Mn_{0.2}O_2$ full cells. The outstanding performance of *β*-fluorinated sulfones designed by applying the “golden middle way” paves a new path for the development of an effective electrolyte system.

Lithium-ion batteries (LIBs) have achieved huge success in the consumer electronics market [1-5] and are currently dominating the energy storage application for the electric vehicles (EVs) market. [4-8] However, it is essential to further increase the energy density of LIBs in order to meet the long-distance transportation requirement of EVs, and thus facilitate their massive commercialization. [9-12] To accomplish this goal, new cathode materials with elevated operating voltage and enhanced specific capacity have been actively pursued. [13-19] Among these new materials, nickel-rich layered oxide cathodes $LiNi_xMn_yCo_zO_2$ are promising candidates owing to their high specific capacity and electrochemical stability at high cutoff voltages. [17-22] Yet, the use of conventional electrolytes, which comprise lithium hexafluorophosphate ($LiPF_6$) dissolved in ethylene carbonate (EC) and ethyl methyl carbonate (EMC) or dimethyl carbonate (DMC), imposes great challenges to the utilization of these cathodes due to the high voltage instability of the electrolytes (Figure S1 depicts the structures of $LiPF_6$ and the solvent molecules used in this study). [21-28] Therefore, new electrolyte systems with improved anodic stability such as super-concentrated electrolytes, [26-31] localized concentrated electrolytes, [32-33], and EC-free electrolytes [34-39] have been proposed. Among the newly proposed electrolytes, fluorination of the ordinary electrolyte solvents provides one of the most promising candidates for high voltage applications [21,23,26,40-43] because the fluorinated substitution group enhances the anodic stability of the molecules, rendering some fluorinated solvents such as fluorinated carbonates and sulfones not only kinetically but also thermodynamically stable towards the high voltage environment. [42-46] Owing to their high anodic stability and reasonable polarity, fluorinated carbonates and sulfones are considered the most promising candidates for high voltage LIBs. [44,45] However, there is no study elucidating the significance of the position of fluorination in those solvent molecules. In this paper, we will not only present the design, synthesis, and successful application of novel *β*–fluorinated sulfones in high voltage LIBs, but also illustrate the importance of the fluorinated position, revealing the "golden middle way" in designing novel fluorinated solvents.

Although the use of α-fluorinated sulfones such as trifluoromethyl ethyl sulfone (FMES) and trifluoromethyl propyl sulfone (FMPS) as electrolyte solvents was demonstrated in a previous study, [46] there has been no study of the structure-activity relationship between fluorinated sulfones and the electrochemical performance of LIBs. In fact, the introduction of a fluorinated group adjacent to the functional group as in α-fluorinated sulfone drastically reduces the polarity of the sulfonyl group, and thus lowers the conductivity of the α-fluorinated sulfone-based electrolyte. On the other hand, the fluorinated group of γ-fluorinated sulfones such as 1,1,1-trifluoro-3-(methylsulfonyl)propane (FPMS) is too distant from the sulfonyl group, imposing an only limited electron withdrawing effect. [46] Figure 1 shows the structures of sulfone molecules with different fluorinated positions. To gain a thorough understanding of the structural effect of fluorinated sulfones, we designed and synthesized β-fluorinated sulfones 1,1,1-trifluoro-2-(methylsulfonyl)ethane (TFEMS) and 1,1,2,2-tetrafluoro-3-(methylsulfonyl)propane (TFPMS), of which the ^{1}H, ^{13}C, and ^{19}F NMR spectra are displayed in Figures S2-S7, respectively, according to Scheme 1. The corresponding alkyl iodides were reacted with sodium methanethiolate to give the thiol intermediates, which were oxidized by hydrogen peroxide to yield the fluorinated sulfones.

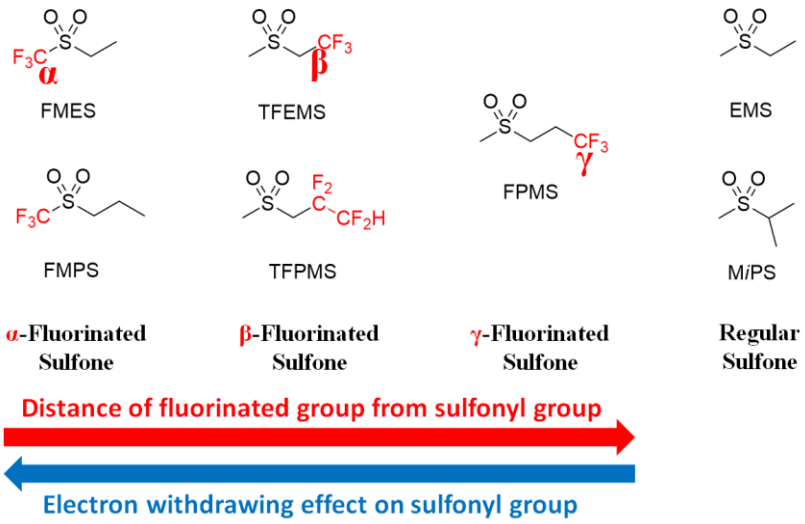

Figure 1. Sulfones with fluorinated group in different position.

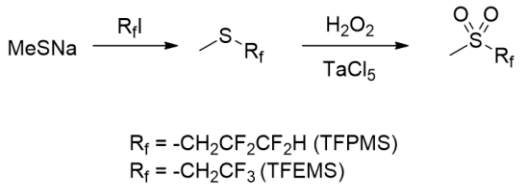

Scheme 1. Synthetic routes for fluorinated sulfones TFEMS and TFPMS.

Density-functional theory calculations were performed to determine both the lowest unoccupied molecular orbital (LUMO) and highest occupied molecular orbital (HOMO) levels of ethyl methyl sulfone (EMS), FMES, TFEMS, FMPS and FEC (Figure S8). Clearly, FMES possesses lowest HOMO level and EMS gives the highest one among all sulfones, while the level of TFEMS lies in the middle. The result indicates FMES has the highest oxidation potential. Meanwhile, the LUMO level of FMES is also the lowest while EMS possesses the highest level, implying the reduction potential of FMES is also the highest. This low cathodic stability of α-fluorinated sulfones is harmful to the graphite anode, as demonstrated by the differential capacity profile and the potentiostatic hold study [47] depicted respectively in Figures 2a and 2b. In our study, β–fluorinated sulfone TFPMS was used exclusively since TFEMS is a solid with a melting point of 60 °C and fluoroethylene carbonate (FEC) was added as a co-solvent to yield a high quality solid electrolyte interphase (SEI) layer. Owing to the low anodic stability of EC, severe electrolyte decomposition and the formation of unstable cathode-electrolyte interphase (CEI) can seriously hamper the cycling performance of high voltage LIBs. [35-36,48] Therefore, FEC was chosen as the SEI enabler since its low solvating power and high anodic stability ensures its minimal contribution to the side reactions on cathode. The differential capacity profiles of Li||graphite half cells employing EMS- and TFPMS-based electrolytes with $LiPF_6$ salt and FEC co-solvent are very similar, while reduction peaks appear around 0.8 V- 0.9 V for the cells using FMES- and FMPS-based electrolytes, indicating severe decomposition of the α-fluorinated sulfones during the charging of graphite.

This severe decomposition may destabilize the SEI layer, leading to reduced discharge capacity. The instability of α-fluorinated sulfones towards the graphite anode was further supported by the study of parasitic reactions of the graphite anode through a leakage current measurement system. [47,49] The static leakage current of Li||graphite cells employing different sulfone-based electrolytes that were placed at a constant temperature of 30 °C was extracted from the current relaxation curve. A typical current relaxation curve was shown in Figure S9. Apparently, the static current of the cell using an FMES-based electrolyte is significantly higher than that of the EMS or TFPMS cell, suggesting that FMES is not as stable as EMS or TFPMS towards the graphite anode.

Apart from the low cathodic stability, α–fluorinated sulfone-based electrolytes also suffer from high flammability and low conductivity. Similar to the 1.2 M $LiPF_6$ in FEC/EMC electrolyte, the 1.2 M $LiPF_6$ in FEC/FMPS electrolyte immediately caught fire on ignition, and the burning was ongoing after the torch was removed, as depicted in Figure S10. In contrast, the TFPMS-based electrolyte did not catch fire at all, and there was no burning after the removal of the torch, implying that TFPMS is a non-flammable solvent. Figure S11 displays the conductivities as a function of temperature of 0.5M $LiPF_6$ in methyl isopropyl sulfone (M*i*PS), TFPMS, and FMPS, which all contain four carbon atoms. Evidently, the conductivity of $LiPF_6$ in regular sulfone M*i*PS is the highest, while the conductivity of the TFMPS-based electrolyte is still significantly higher than that of the FMPS electrolyte. The temperature dependence of the conductivity can be described by the VTF (Vogel–Tamman–Fulcher) empirical equation described in Table S1, which also summarizes the fitting parameters for sulfone-based electrolytes, [50] while Figures S12-S14 present the VTF fitting curves of respectively 0.5 M $LiPF_6$ FMPS, TFPMS, and M*i*PS electrolytes, respectively. In the VTF equation, σ is the conductivity of the electrolyte, σ_0 is the pre-exponential factor, T_0 represents the glass transition temperature, T represents the absolute temperature, and B is related to the activation energy of ion transport associated with the configurational entropy of the electrolyte. The M*i*PS electrolyte possesses the highest conductivity due to its high polarity, while the

conductivity of the FMPS electrolyte is the lowest. Moreover, the activation energies of these electrolytes also follow the same trend, with the M*i*PS electrolyte displaying the highest activation energy and FMPS electrolyte showing the lowest one. Clearly, both the conductivity and activation energy of the TFPMS electrolyte lie in the middle of those of the M*i*PS and FMPS electrolytes.

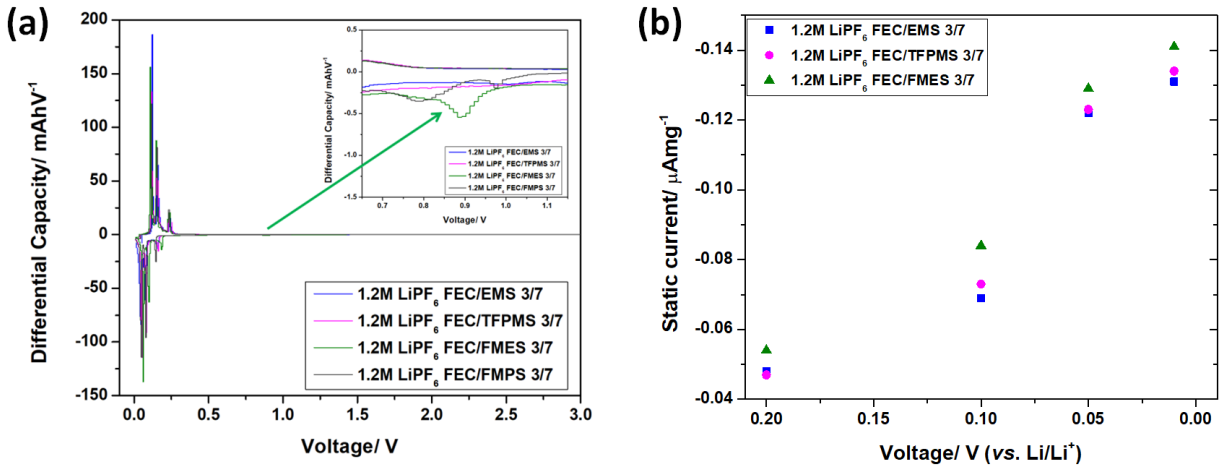

Figure 2. (a) Differential capacity profile of Li||graphite half cells with 1.2M $LiPF_6$ FEC/EMS 3/7, FEC/TFPMS 3/7, and FEC/ FMES 3/7 electrolytes and (b) variation of the static leakage current as a function of potential for different sulfone-based electrolytes in Li||graphite cells.

To assess the anodic stability of the electrolyte solvent, which is highly important for the operation of high density, high voltage lithium batteries, [23,44-46] linear sweep voltammetry (LSV) measurements were conducted, and the results are presented in Figure S15. The electrolytes contained 0.5 M $LiPF_6$ dissolved in corresponding sulfones due to the limited solubility of FMPS. Apparently, the onset voltages of all fluorinated sulfone-based electrolytes are higher than their non-fluorinated counterparts, indicating an increase in the oxidation stability of the solvents. The onset potential of the anodic current for the oxidation of the M*i*PS electrolyte is at 6.0 V, which is smaller than that of the EMS electrolyte (6.2 V). The onset voltage for the TFPMS electrolyte is at 6.8 V, which is lower than that of the FMPS (its corresponding α–fluorinated sulfone) electrolyte. This is reasonable because the highly electron withdrawing fluorinated group is one carbon atom farther away from the sulfonyl group in TFPMS

compared to FMPS. Thus, the anodic stability of β–fluorinated sulfone lies in between that of α–fluorinated sulfone and regular sulfone, displaying again the middle ground property of β–fluorinated sulfone.

Multi-nuclear magnetic resonance (NMR) techniques were deployed to reveal the lithium solvating ability of the sulfone molecules, [51-52] which is another critical property determining the cycling stability of a lithium cell employing a sulfone-based electrolyte. [532] To evaluate and compare the lithium solvating abilities of individual sulfones, we measured their relative solvating power (χ), which is the ratio of the coordination percentage of a sulfone to the coordination percentage of EMC, which is used as the reference solvent. [52] Figure S16 depicts the Fourier-transform infrared (FTIR) spectra of EMC, TFPMS, and $LiPF_6$:TFPMS:EMC 1:4:4 (molar ratio) solutions. The coordination ratio of EMC can be easily deconvoluted due to its distinctive carbonyl absorption peak. As presented in Figure S17, the deconvoluted coordination percentages of EMC in $LiPF_6$:FMES:EMC, $LiPF_6$:FMPS:EMC, and $LiPF_6$:TFPMS:EMC solutions are 65 %, 65 % and 58 %, respectively, implying β–fluorinated sulfone possesses a higher lithium solvating ability than α–fluorinated sulfone. Unfortunately, the absorption peaks of fluorinated sulfones are severely overlapping with those of EMC and $LiPF_6$, rendering any meaningful deconvolution impossible. Yet, internally referenced diffusion-ordered spectroscopy (IR-DOSY) provides a feasible way to determine the solvation states of TFPMS, since the proton peaks of TFPMS are distinctive from those of EMC in the ^{1}H-NMR spectrum of $LiPF_6$:EMC:TFPMS solution (Figure S18). [51-52] Figures S19 and S20 display respectively the ^{1}H-NMR spectra of $LiPF_6$:EMC:FMES and $LiPF_6$:EMC:FMPS solutions. Obviously, the absorption peaks from fluorinated sulfone can be easily distinguished from the peaks of EMC and toluene, which is used as an internal reference. Figures 3a and 3b illustrate respectively the ^{1}H DOSY spectra of EMC:TFPMS 1:1 and $LiPF_6$:EMC:TFPMS 1:4:4 solutions. Before the addition of $LiPF_6$, EMC diffuses significantly faster than TFPMS due to its smaller size. However, the diffusion coefficient of EMC reduces drastically after the

addition of $LiPF_6$ and is very similar to that of TFPMS, indicating that EMC has the stronger lithium solvating ability. Table S2 summarizes the diffusion coefficients and coordination ratios of EMC and TFPMS, as well as the coordination number of lithium in 1:4:4 $LiPF_6$:EMC:TFPMS electrolyte. Subsequently, the solvation states of FMES and FMPS were also determined by IR-DOSY (Figures S21 and S22, respectively,) and the results are also respectively summarized in Tables S3 and S4. After obtaining the coordination percentages of TFPMS, FMES, and FMPS relative to EMC, the relative solvating power (χ) of the sulfones can be obtained by calculating the ratio of the coordination percentage of the sulfone to the coordination percentage of EMC. Clearly, the lithium solvating ability of α–fluorinated sulfone is significantly smaller than that of β–fluorinated sulfone. Figure S23 depicts the solvating power series of common electrolyte solvents with FMPS, FMES, TFPMS, and EMS. [53] The lithium solvating ability of both α–fluorinated sulfone and β–fluorinated sulfone is significantly smaller than that of EMC, while the solvating power of regular sulfone is notably larger than that of EMC. Although the solvating power of TFPMS is larger than that of α–fluorinated sulfone, it is very similar to the solvating ability of trifluoroethyl methyl carbonate (FEMC), which has been shown as a potential electrolyte solvent enhancing the cycling performance of high voltage LIBs. [44-45]

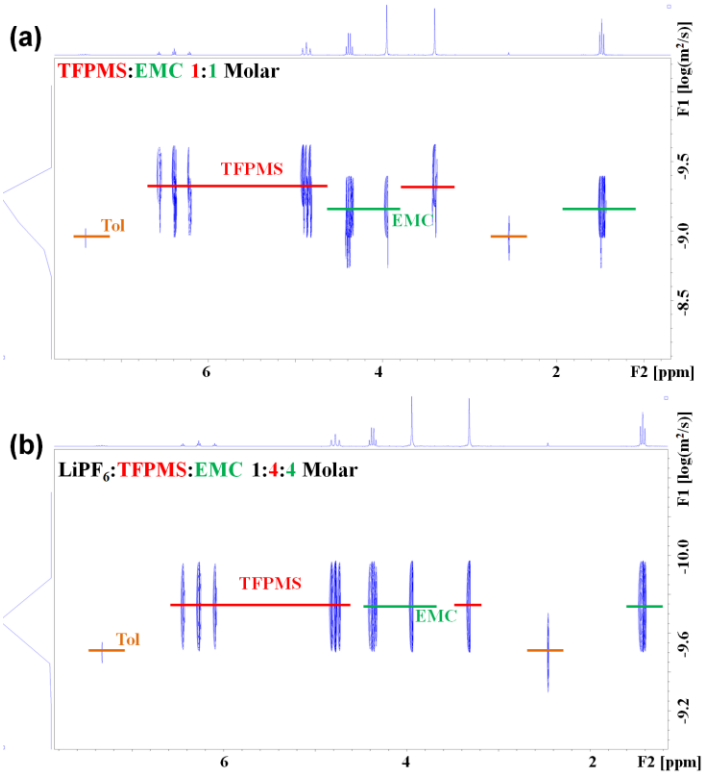

Figure 3. ^{1}H DOSY-NMR spectra of (a) 1:1 (molar ratio) EMC:TFPMS and (b) 1:4:4 $LiPF_6$:EMC:TFPMS electrolyte with toluene added as an internal reference.

The importance of the middle ground properties for the *β*–fluorinated sulfone TFPMS is demonstrated by the electrochemical performance of graphite||$LiNi_{0.6}Co_{0.2}Mn_{0.2}O_2$ (NMC622) full cell cycling at a rate of C/2 between 3.0 V and 4.5 V. Figures 4a and S24 illustrate the capacity retention and Coulombic efficiency (CE) of graphite||NMC622 cells using the conventional EC-based electrolyte (Gen2, 1.2 M $LiPF_6$, plus EC/EMC) and 1.2 M $LiPF_6$ dissolved in FEC and various co-solvents, while Table S5 summarizes the cycling details including the 1st CE, 1st cycle capacity, and capacity retention (CR) after 400 cycles and the average capacity (AC) across 400 cycles. The cells employing EMC-based (EC/EMC and FEC/EMC) electrolytes displayed 66% CR after 400 cycles, which is significantly higher than the CR of cells using the EMS-based electrolyte (48%). However, the CRs after 400 cycles for all fluorinated sulfone cells are larger than 71%, demonstrating the effectiveness of fluorinated sulfones in improving the

cycling performance of full cells. The 1st CEs of FMES and FMPS cells are significantly lower than that of TFPMS cells due to the decomposition of α–fluorinated sulfones on graphite anodes, as discussed above. Overall, the TFPMS cells displayed the highest CR (81%) and AC (168 mAh/g) after 400 cycles among all the cells. To further verify the advantage of β–fluorinated sulfone, difluoroethylene carbonate (DFEC) was also used as the SEI enabler. The capacity retention and CE of graphite||NMC622 cells employing DFEC/sulfone electrolytes are depicted in Figures 4b and S25 respectively, and the details of cycling are summarized in Table S6. Again, the cell showing the highest AC was the TFPMS cell, which is 161 mAh/g. Moreover, the TFPMS cells displayed the lowest polarization after 400 cycles, evidenced by the 400th cycle voltage profiles of the full cells using FEC-based and DFEC-based electrolytes depicted respectively in Figures S26a and S26b. As illustrated in Figure S27, the graphite|| $LiNi_{0.8}Co_{0.1}Mn_{0.1}O_2$ full cell adopting FEC-TFPMS electrolyte also displayed enhanced capacity and CE compared to the EMS and FMES cells even at high temperature (50 ^{o}C). Although the defluorination of FEC that led to the formation of lithium fluoride is believed to further stabilize the SEI on graphite anode at high temperature, [54] the performance of EMS cell was still much worse than the TFPMS cell, probably due to the high solvating ability of EMS. [53] Altogether, the middle ground properties of TFPMS facilitate the stable cycling of the graphite||NMC full cell with high enough anodic stability, but relatively low reduction potential and lithium solvating power.

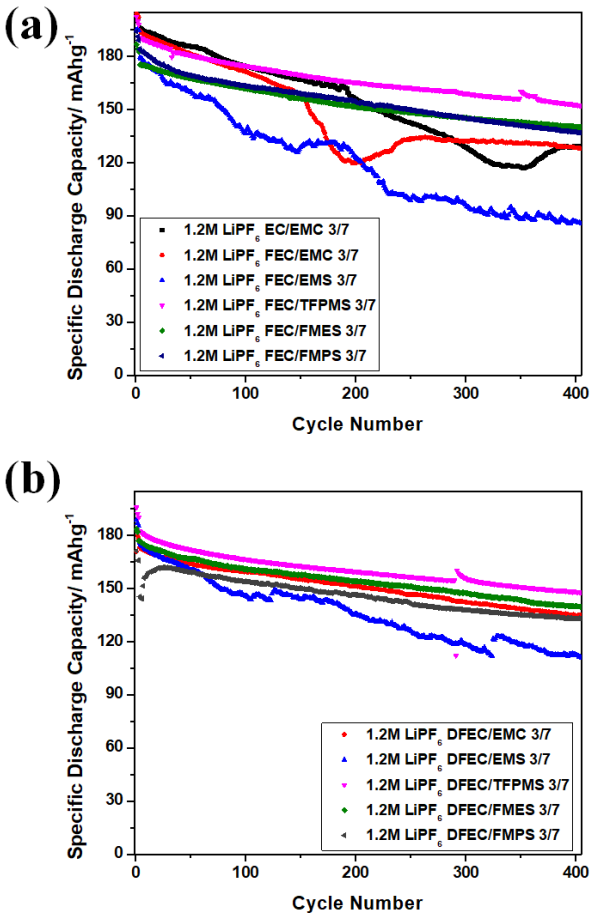

Figure 4. Cycling performance of graphite||NMC622 cells using (a) 1.2 M $LiPF_6$ plus EC/EMC (Gen2), FEC/EMC, FEC/EMS, FEC/TFMPS, FEC/FMES, and FEC/FMPS electrolytes (3/7 volume ratios); (b) 1.2 M $LiPF_6$ plus DFEC/EMC, DFEC/EMS, DFEC/TFMPS, DFEC/FMES, and DFEC/FMPS electrolytes (3/7 volume ratios) at room temperature.

The extent of transition metal (TM) dissolution from the NMC622 cathode was also examined, and the amounts of Co, Mn, and Ni dissolved in the electrolytes and deposited on the harvested graphite of the graphite||NMC622 cells using different electrolytes were quantified by inductively coupled plasma mass spectrometry (ICP-MS). Figure S28 shows the amounts of TM deposited on the harvested graphite anodes of full cells employing FEC/EMC, FEC/EMS, and FEC/TFPMS electrolytes after 400 cycles. Apparently, the TM dissolution and deposition is most severe in the EMS cell due to the high lithium solvating power of EMS. [53] In contrast, the total amount of TM deposition on the graphite of the TFPMS cell was not

only the lowest, but was also significantly lower than that of the EMC cell because of the high anodic stability and relatively mild lithium solvating power of TFPMS. The same trend was obtained for the full cells employing DFEC-based electrolytes. As depicted in Figure S29, the total amount of TM deposition on the graphite of DFEC/EMS cell was noticeably higher than that of the DFEC/TFPMS cell. These results clearly suggest that the *β*–fluorinated sulfone-based electrolyte can better mitigate TM dissolution and deposition compared to the regular sulfone-based electrolyte, leading to a remarkable improvement in cycling performance.

All in all, we designed and synthesized a new class of electrolyte solvents, *β*-fluorinated sulfones, for high voltage LIBs through the "golden middle way" principle. Although *β*-fluorinated sulfone (TFPMS) does not possess the "best" quality of any single electrochemical property, such as conductivity and anodic stability, its "just enough" feature renders the best cycling performance of graphite||NMC622 high voltage cells using the TFPMS-based electrolyte. Since the highly electron withdrawing fluorinated group is one carbon atom farther away from the sulfonyl group in TFPMS compared the *α*-fluorinated sulfones, TFPMS possesses a slightly lower anodic stability than *α*-fluorinated sulfones. However, its anodic stability is still significantly higher than that of the regular sulfone (EMS), making it resistant to oxidation on the high voltage NMC622 cathode. Owing to their high reduction potentials, *α*-fluorinated sulfones easily decompose on graphite anodes, leading to very low 1^{st} cycle CEs for the graphite||NMC622 employing FMPS- or FMES-based electrolytes. In contrast, the lowered reduction potential of TFPMS renders it stable towards the graphite anode that result in a much higher 1^{st} cycle CE for the TFPMS cell. Moreover, unlike FMES and FMPS, TFPMS is a non-flammable solvent. Compared to regular sulfone (EMS), the solvating power of TFPMS is much reduced, mitigating the TM dissolution of the NMC622 cathode. Taken together, the middle ground properties of the newly synthesized *β*-fluorinated sulfone facilitate highly stable cycling of high voltage graphite||NMC full cells.

ASSOCIATED CONTENT

Supporting Information

Experimental section, NMR data, FTIR data, Raman data, and density-functional theory calculation. This material is available free of charge via the Internet.

AUTHOR INFORMATION

Corresponding Authors

*Email: amine@anl.gov; csu@anl.gov; mhe@wpi.edu

Conflicts of interest

There are no conflicts of interest to declare.

ACKNOWLEDGMENTS

The authors gratefully acknowledge support from the U.S. Department of Energy (DOE), Vehicle Technologies Office (VTO). Argonne National Laboratory is operated by DOE Office of Science by UChicago Argonne, LLC, under contract number DE-AC02-06CH11357. The NMC electrodes were manufactured at the DOE's CAMP Facility, at Argonne National Laboratory. The CAMP Facility is fully supported by the DOE VTO within the core funding of the Applied Battery Research for Transportation Program. The authors also thank K. Pupek and G. Krumdick from Argonne's Materials Engineering Research Facility for providing FMES and FMPS.

REFERENCES

1. Tarascon, J.-M.; Armand, M., *Nature* **2001**, *414*, 359.
2. Armand, M.; Tarascon, J.-M., *Nature* **2008**, *451*, 652.
3. Goodenough, J. B.; Park, K.-S., *J. Am. Chem. Soc.* **2013**, *135*, 1167.

4. Li, M.; Lu, J.; Chen, Z.; Amine, K., *Adv. Mater.* **2018**, e1800561.
5. Weiss, M.; Simon, F. J.; Busche, M. R.; Nakamura, T.; Schröder, D.; Richter, F. H.; Janek, J., *Electrochem. Energy Rev.* **2020**, *3*, 221.
6. Nitta, N.; Wu, F.; Lee, J. T.; Yushin, G., Li-Ion Battery Materials: Present and Future. *Mater. Today* **2015**, *18* (5), 252.
7. Wang, C.; Adair, K. R.; Liang, J.; Li, X.; Sun, Y.; Li, X.; Wang, J.; Sun, Q.; Zhao, F.; Lin, X.; Li, R.; Huang, H.; Zhang, L.; Yang, R.; Lu, S.; Sun, X., *Adv. Funct. Mater.* **2019**, *29*, 1900392.
8. Zhu, Y.-H.; Zhang, Q.; Yang, X.; Zhao, E.-Y.; Sun, T.; Zhang, X.-B.; Wang, S.; Yu, X.-Q.; Yan, J.-M.; Jiang, Q., *Chem* **2019**, *5*, 168.
9. Lin, F.; Markus, I. M.; Nordlund, D.; Weng, T.-C.; Asta, M. D.; Xin, H. L.; Doeff, M. M., *Nat. Commun.* **2014**, *5*, 3529.
10. Schmuch, R.; Wagner, R.; Hörpel, G.; Placke, T.; Winter, M., *Nat. Energy* **2018**, *3*, 267.
11. Li, G.; Liao, Y.; Li, Z.; Xu, N.; Lu, Y.; Lan, G.; Sun, G.; Li, W., *ACS Appl. Mater. & Interfaces* **2020**, *12* (33), 37013.
12. Hu, S.; Pillai, A. S.; Liang, G.; Pang, W. K.; Wang, H.; Li, Q.; Guo, Z., *Electrochem. Energy Rev.* **2019**, *2*, 277.
13. Wu, F.; Li, W.; Chen, L.; Su, Y.; Bao, L.; Bao, W.; Yang, Z.; Wang, J.; Lu, Y.; Chen, S., *Energy Storage Mater*. **2020**, *28*, 383.
14. Santhanam, R.; Rambabu, B., *J. Power Sources* **2010**, *195*, 5442.
15. Hu, M.; Pang, X.; Zhou, Z., *J. Power Sources* **2013**, *237*, 229.
16. Liu, S.; Xiong, L.; He, C., *J. Power Sources,* **2014**, *261*, 285.
17. Lin, F.; Markus, I. M.; Nordlund, D.; Weng, T.-C.; Asta, M. D.; Xin, H. L.; Doeff, M. M., *Nat. Commun.* **2014,** *5*, 3529.
18. Ohzuku, T.; Makimura, Y., *Chem. Lett.* **2001,** *7*, 642–643.
19. Li, W.; Song, B.; Manthiram, A., *Chem. Soc. Rev.* **2017**, *46* (10), 3006.
20. Xu, J.; Lin, F.; Doeff, M. M.; Tong, W., *J. Mater. Chem. A* **2017**, *5* (3), 874.
21. He, M.; Su, C.-C.; Feng, Z.; Zeng, L.; Wu, T.; Bedzyk, M. J.; Fenter, P.; Wang, Y.; Zhang, Z.,

Adv. Energy Mater. **2017**, *7* (15), 1700109.

22. Su, C. C.; He, M.; Peebles, C.; Zeng, L.; Tornheim, A.; Liao, C.; Zhang, L.; Wang, J.; Wang, Y.; Zhang, Z., *ACS Appl. Mater. & Interfaces* **2017**, *9* (36), 30686.
23. Xu, K., *Chem. Rev.*, **2014**, *114*, 11503.
24. Xu, M.; Zhou, L.; Dong, Y.; Chen, Y.; Demeaux, J.; Macintosh, A. D.; Garsuch, A.; Lucht, B. L., *Energy Environ. Sci.*, **2016**, *9*, 1308.
25. Xia, J.; Petibon, R.; Xiong, D.; Ma, L.; Dahn, J., *J. Power Sources* **2016,** *328*, 124.
26. Chen, S.; Wen, K.; Fan, J.; Bando, Y.; Golberg, D., *J. Mater. Chem. A* **2018**, *6* (25), 11631.
27. Zheng, J.; Lochala, J. A.; Kwok, A.; Deng, Z. D.; Xiao, J., *Adv. Sci.* **2017**, *4* (8), 1700032.
28. Yamada, Y.; Wang, J.; Ko, S.; Watanabe, E.; Yamada, A., *Nat. Energy* **2019**, *4* (4), 269.
29. Alvarado, J.; Schroeder, M. A.; Zhang, M.; Borodin, O.; Gobrogge, E.; Olguin, M.; Ding, M. S.; Gobet, M.; Greenbaum, S.; Meng, Y. S.; Xu, K., *Mater. Today* **2018**, *21* (4), 341.
30. Wang, J.; Yamada, Y.; Sodeyama, K.; Watanabe, E.; Takada, K.; Tateyama, Y.; Yamada, A., *Nat. Energy* **2017**, *3* (1), 22.
31. Wang, J.; Yamada, Y.; Sodeyama, K.; Chiang, C. H.; Tateyama Y.; Yamada, A., *Nat. Commun*. **2016**, *7*, 2032.
32. Jia, H.; Zou, L.; Gao, P.; Cao, X.; Zhao, W.; He, Y.; Engelhard, M. H.; Burton, S. D.; Wang, H.; Ren, X.; Li, Q.; Yi, R.; Zhang, X.; Wang, C.; Xu, Z.; Li, X.; Zhang, J. G.; Xu, W., *Adv. Energy Mater*. **2019**, *9* (31), 1900784.
33. Chen, S.; Zheng, J.; Mei, D.; Han, K. S.; Engelhard, M. H.; Zhao, W.; Xu, W.; Liu, J.; Zhang, J. G., *Adv. Mater.* **2018**, *30* (21), e1706102.
34. Logan, E. R.; Dahn, J. R., *Trends Chem.* **2020**, *2* (4), 354.
35. Xia, J.; Petibon, R.; Xiong, D.; Ma, L.; Dahn, J. R., *J. Power Sources* **2016**, *328*, 124.
36. Li, W.; Dolocan, A.; Li, J.; Xie, Q.; Manthiram, A., *Adv. Energy Mater* **2019**, *9* (29), 1901152.
37. Ehteshami, N.; Ibing, L.; Stolz, L.; Winter, M.; Paillard, E., *J. Power Sources* **2020**, *451*, 227804.

38. Yu, Y.; Huang, G.; Du, J.-Y.; Wang, J.-Z.; Wang, Y.; Wu, Z.-J.; Zhang, X.-B., *Energy Environ. Sci.* **2020**, *13*, 3075.

39. Yu, Y.; Zhang, X.-B., *Matter* **2019**, *1*, 881.

40. Yu, Z.; Wang, H.; Kong, X.; Huang, W.; Tsao, Y.; Mackanic, D. G.; Wang, K.; Wang, X.; Huang, W.; Choudhury, S.; Zheng, Y.; Amanchukwu, C. V.; Hung, S. T.; Ma, Y.; Lomeli, E. G.; Qin, J.; Cui, Y.; Bao, Z., *Nat. Energy* **2020**, *5*, 526.

41. Fan, X.; Chen, L.; Borodin, O.; Ji, X.; Chen, J.; Hou, S.; Deng, T.; Zheng, J.; Yang, C.; Liou, S. C.; Amine, K.; Xu, K.; Wang, C., *Nat. Nanotechnol.* **2018**, *13* (8), 715.

42. von Aspern, N.; Roschenthaler, G. V.; Winter, M.; Cekic-Laskovic, I., *Angew. Chem. Int. Ed.* **2019**, *58* (45), 15978.

43. Chen, L.; Fan, X.; Hu, E.; Ji, X.; Chen, J.; Hou, S.; Deng, T.; Li, J.; Su, D.; Yang, X.; Wang, C., *Chem* **2019**, *5* (4), 896.

44. He, M.; Hu, L.; Xue, Z.; Su, C. C.; Redfern, P.; Curtiss, L. A.; Polzin, B.; von Cresce, A.; Xu, K.; Zhang, Z., *J. Electrochem. Soc.* **2015**, *162* (9), A1725.

45. Zhang, Z.; Hu, L.; Wu, H.; Weng, W.; Koh, M.; Redfern, P. C.; Curtiss, L. A.; Amine, K., *Energy Environ. Sci.* **2013**, *6* (6), 1806.

46. Su, C.-C.; He, M.; Redfern, P. C.; Curtiss, L. A.; Shkrob, I. A.; Zhang, Z., *Energy Environ. Sci.* **2017**, *10* (4), 900.

47. Gao, H.; Xiao, L.; Plumel, I.; Xu, G. L.; Ren, Y.; Zuo, X.; Liu, Y.; Schulz, C.; Wiggers, H.; Amine, K.; Chen, Z., *Nano lett.* **2017**, *17* (3), 1512.

48. Xu, M.; Zhou, L.; Dong, Y.; Chen, Y.; Demeaux, J.; MacIntosh, A. D.; Garsuch, A.; Lucht, B. L., *Energy Environ. Sci.* **2016**, *9*, 1308.

49. Zeng, X.; Xu, G.-L.; Li, Y.; Luo, X.; Maglia, F.; Bauer, C.; Lux, S. F.; Paschos, O.; Kim, S.-J.; Lamp, P.; Lu, J.; Amine, K.; Chen, Z., *ACS Appl. Mater. & Interfaces* **2016**, *8* (5), 3446.

50. Elia, G. A.; Ulissi, U.; Jeong, S.; Passerini, S.; Hassoun, J., *Energy Environ. Sci.* **2016**, *9* (10), 3210.

51. Su, C. C.; He, M.; Amine, R.; Chen, Z.; Amine, K., *J. Phys. Chem. Lett.* **2018**, *9* (13), 3714.

52. Su, C.-C.; He, M.; Amine, R.; Rojas, T.; Cheng, L.; Ngo, A. T.; Amine, K., *Energy Environ. Sci.* **2019**, *12*, 1249.
53. Su, C. C.; He, M.; Amine, R.; Chen, Z.; Amine, K., *Nano Energy* **2021**, *83*, 105843.
54. He, M.; Su, C.-C.; Peebles, C.; Zhang, Z., *J. Electrochem. Soc.* **2021**, *168*, 010505.

KEYWORDS

High voltage lithium-ion batteries, high voltage electrolytes, non-flammable electrolytes, design of electrolyte molecules, electrolyte solvation

Undoubtedly, it is not an easy task to design and synthesize new molecule that can be applied as electrolyte solvent. What's more, researchers usually focused only on one particular property and ended up synthesizing molecules that are outstanding in that property while overlooking the other equally important features that might be essential for the stable cycling of lithium-ion batteries. For example, α-fluorinated sulfones possess outstanding anodic stability, since the strong electron withdrawing trifluoromethyl group is directly attached to the sulfonyl group. However, such a strong electron withdrawing effect significantly increases the reduction potential of α-fluorinated sulfones, rendering them unstable towards graphite anodes. In this study, we introduce a "golden middle way" in designing and synthesizing new electrolyte solvents. With the trifluoromethyl group located on the β position, the newly synthesized β-fluorinated sulfone (TFPMS) is not only oxidatively stable enough to withstand the high voltage NMC622 cathode but also reductively stable towards the graphite anode. Overall, TFPMS is not the best in any one particular property, but its "middle ground" properties successfully enable very stable long cycling of high voltage graphite||NMC622 full cells.